ACS chemical biology

Letters

pubs.acs.org/acschemicalbiology

Determination of the Formylglycinamide Ribonucleotide Amidotransferase Ammonia Pathway by Combining 3D-RISM Theory with Experiment

Ajay S. Tanwar,[†,§] Daniel J. Sindhikara,[‡,§,∥] Fumio Hirata,*[,‡] and Ruchi Anand*[,†]

[†]Department of Chemistry, Indian Institute of Technology, IIT-Bombay, Mumbai 400076, India

[‡]College of Life Sciences, Ritsumeikan University and Molecular Design Frontier Co. Ltd., Kyoto, Japan

Supporting Information

ABSTRACT: Molecular tunnels in enzyme systems possess variable architecture and are therefore difficult to predict. In this work, we design and apply an algorithm to resolve the pathway followed by ammonia using the bifunctional enzyme formylglycinamide ribonucleotide amidotransferase (FGAR-AT) as a model system. Though its crystal structure has been determined, an ammonia pathway connecting the glutaminase domain to the 30 Å distal FGAR/ATP binding site remains elusive. Crystallography suggested two purported paths: an N-terminal-adjacent path (path 1) and an auxiliary ADP-adjacent path (path 2). The algorithm presented here, *RismPath*, which enables fast and accurate determination of solvent distribution inside a protein channel, predicted path 2 as the preferred mode of ammonia transfer. Supporting experimental studies validate the identity of the path, and results lead to the conclusion that the residues in the middle of the channel do not partake in catalytic coupling and serve only as channel walls facilitating ammonia transfer.

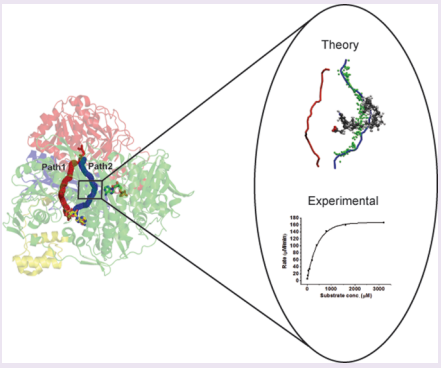

When two active sites that carry diverse reactions are connected via a tunnel or channel by which the product produced in one active center is transferred to the other active site for subsequent catalysis, substrate channelling occurs.[1−4] Substrate channelling happens when the products require (a) protection from decomposition by the aqueous external environment,[2] (b) enhanced catalysis,[3] (c) reduced transient time, etc.[3] Since ammonia is a reactive intermediate and can readily get protonated in an aqueous environment, yielding ammonium ions, in most cases it is transferred via an internal tunnel to a second catalytic domain or subunit, where it can perform a nucleophilic attack on a substrate.[5] The ammonia produced in these enzyme systems is derived from the amide moiety of glutamine and generated by amidotransferase (AT) domains.[5,6] The AT superfamily is widespread and participates in several metabolic pathways. It encompasses two major types of glutaminases: type I employs a N-terminal cysteine residue for hydrolysis of glutamine,[7] whereas in type II, this cysteine is a part of a catalytic triad.[4,7] Unlike enzyme active sites, molecular tunnels have variable architecture, and residues lining them are generally not conserved even among enzymes catalyzing the same set of reactions. Some of the enzymes like phosphoribosyl pyrophosphate amidotransferase (PurF) represent dynamic ones,[8] and others like carbamoyl phosphate synthetase (CPS) possess permanent channels.[2,9] In several of these cases, both catalytic coupling and intramolecular signaling are observed during the transfer of the unstable intermediate between the two physically separated active centers. This ensures that no wasteful production of ammonia occurs in the absence of the corresponding substrate.[2,6,10−13]

The nature of the residues lining the ammonia varies dramatically from system to system. For example, the intramolecular tunnel of PurF, is hydrophobic in nature,[14] whereas in CPS, it is hydrophilic in nature.[1] Therefore, it is difficult to utilize the information obtained from various well characterized ammonia channelling systems to design a common strategy for pathway elucidation. In such circumstances, a combination of computational and experimental methods can be utilized to identify these tunnels. A key benefit of computational methods is the ability to offer spatial resolution that experimental methods cannot. But computational methods can be prone to significant errors, including in modeling, force fields, and sampling. For the computation of solvent, two classes of computational solvation are commonly employed: implicit and explicit. Implicit solvent models yield instantaneous relaxation of the solvent, but since they inherently lack microscopic detail, they can lose significant accuracy. Conversely, explicit solvent models may include a microscopic picture, but the added terms in the calculation greatly increase the sampling load. This load must be overcome by extensive molecular dynamics (MD) or grand canonical Monte Carlo (GCMC) calculations. For systems where the

Received: August 28, 2014
Accepted: December 31, 2014
Published: December 31, 2014

DOI: 10.1021/cb501015r
ACS Chem. Biol. 2015, 10, 698−704

Scheme 1. Conversion of FGAR to FGAM

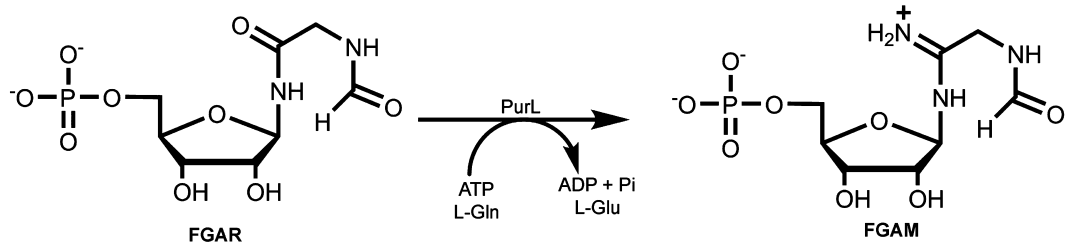

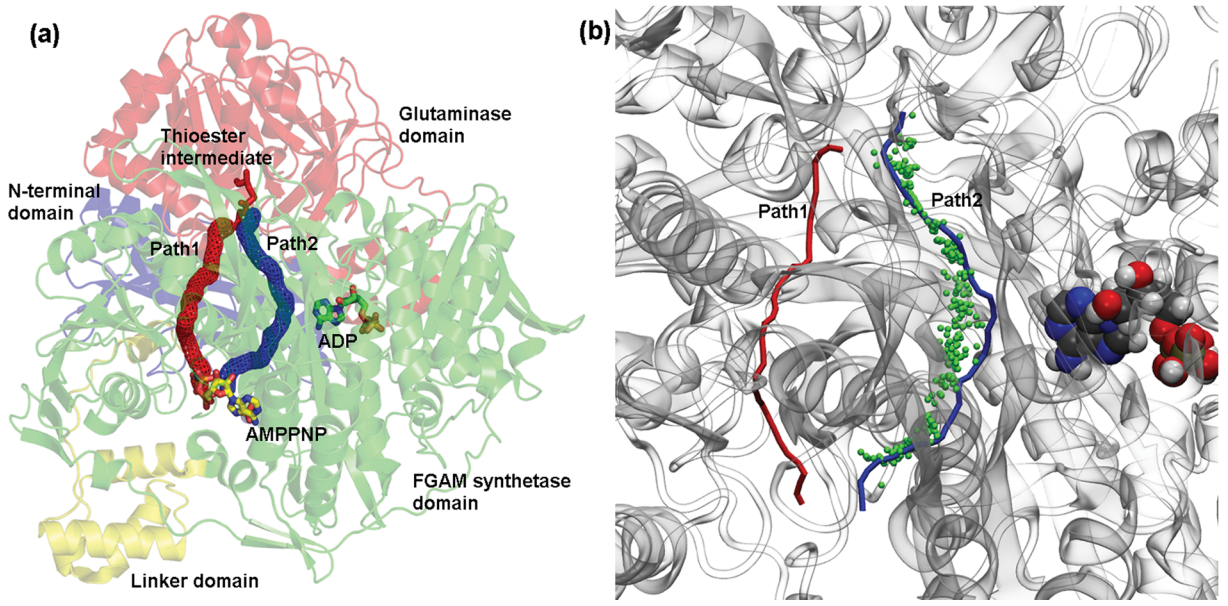

Figure 1. Ammonia channel in StPurL. (a) Two predicted pathway for ammonia channel in StPurL shown in red and blue color mesh for path 1 and path 2, respectively. StPurL structure is depicted as a cartoon with the N-terminal domain in blue, linker domain in yellow, glutaminase domain in red, and FGAM synthetase domain in green color. Ligands are shown in stick representation. (b) Results of *RismPath* calculations on PurL WT trajectory. Crystallography purported path 1 (red) and path 2 (blue) are shown as tubes inside PurL (cartoon, translucent).

solvent configurational space is strictly limited or uniform (bulk-like), or if the channel structure is relatively simple, these explicit solvent sampling schemes work well, but for more complicated cases, such as inside the complex interior of a protein, the sampling is severely frustrated. The problem becomes even more difficult when one has to handle a liquid mixture or solution as in the case of an ammonia channel, in which the affinity of ammonia to the channel pore is determined not just by ammonia itself but also by competing effect with water.

One way to simplify the system is to simply treat the solvent as a van der Waals probe such as is used in the pathway determination algorithms CAVER[15] and MOLE.[16] Another faster algorithim that also utilizes geometric criteria representing molecular channels via construction of corridor trees, MolAxis[17] has also been tested on several membrane channels and enzyme cavities. However, this simplified approximation ignores many important effects such as solvent geometry, electrostatic effects, and solvent−solvent interaction and thus cannot possibly produce a realistic equilibrium distribution. It may be the reason why no successful study has been reported based on the computational methods listed above to identify the ammonia channel under concern. In several cases, molecular dynamics (MD) simulations either alone or in conjunction with other methods have been employed.[18] In particular, ammonia channels in CPS and HisHF have been mapped using MD;[19,20] however due to the high computational expense during MD runs, only a small part of the channel was investigated. Therefore, in the present study, we have decided to apply the 3D-RISM/RISM method to this problem.

The 3D-RISM/RISM is an integral equation method for resolving the solvent distribution, correlations, and related properties in the presence of a solute.[21,22] Analogous to implicit solvation models, a single calculation yields equilibrium results. Similar to explicit solvent simulations, the calculation explicitly includes microscopic effects of water as characterized by atomic solvent models (such as TIP3P or SPC/e).[23,24] Thus, for systems with a complex solvation landscape, 3D-RISM can be ideal for rapidly obtaining converged, detailed solvent data.

In this work to identify a molecular pathway through which ammonia is channelled, we developed a method utilizing 3D-RISM/RISM calculations of the 140 kDa FGAR-AT protein from *Salmonella typhimurium* (also known as StPurL). StPurL catalyzes the fourth step of the purine biosynthetic pathway where FGAR is converted into FGAM in an ATP assisted reaction (Scheme 1). The crystal structure of StPurL was instrumental in deciphering the domain organization of this class of proteins.[25] In all the reported structures of StPurL, the enzyme was found to be trapped in an inactive state with the thioester intermediate bound to the glutaminase active site, and the two active centers were found to be separated by 30 Å.[25]

DOI: 10.1021/cb501015r
ACS Chem. Biol. 2015, 10, 698−704

Previous attempts have been made to find the path traversed by ammonia; however no paths that were completely connecting the two were found.[25] Two plausible pathways were proposed based on the available space in the protein designated as path 1 and path 2 (Figure 1a). Path 1 is sandwiched between the N-terminal and the FGAM synthetase domain interface and is more hydrophilic and shorter in length. However, path 2 is more hydrophobic and passes through the central barrel formed by the two gene-duplicated halves of the FGAM synthetase domain and is near the auxiliary ADP binding site. Recent studies revealed that binding of FGAR is most likely the trigger,[26] which induces the conformational switch necessary for catalysis and formation of the tunnel. In addition, xenon binding studies have shown that in the crystallographically trapped conformation both the proposed paths are inaccessible to external hydrophobic moieties.[27] For the computational study, the crystal structure was taken as an initial model for a MD cascade to introduce fluctuations in the protein. Snapshots from the MD were then analyzed by 3D-RISM, and a path-searching algorithm to identify which of the two proposed paths, path 1 or path 2, is preferred was determined. Further computational blocking mutations were performed along the resulting hypothetical path to evaluate the effectiveness of these mutations. Supporting experimental mutations were designed to validate these results by either constricting or widening the proposed path. Together, investigation of the variant forms of the protein generated via crystallographic, biochemical, and thermal stability studies was utilized to provide critical insights into the path followed by ammonia.

In short, the 3D-RISM and 1D-RISM are based on the site-based interpretation of the molecular Ornstein−Zernike equation.[28]

$$h(12) = c(12) + \frac{\rho}{\Omega}\int c(12)\, h(32)\, \mathrm{d}(3)$$

Here, h and c are the total and direct correlation functions, respectively. 1 and 2 represent the coordinates of molecules 1 and 2, and 3 represents a third molecule integrated over all space $\int \mathrm{d}(3)$. ρ represents the solvent density, and Ω is the normalization constant for the angular space. Both 1D and 3D-RISM utilize classical atomic interaction potentials and closure approximations such as the KH closure used here.[29,30] 1D-RISM often utilizes rigid solvent structure, orientational averaging, and dielectric constraints for expedited convergence.[31,32] To model a solvated biomolecular system with 3D-RISM, first 1D-RISM must be performed on the solvent mixture to obtain the solvent correlation functions. These solvent data, in combination with the solute biomolecular structure and parameters, are then input into the 3D-RISM calculation which is then iterated until convergence. The result of this calculation is the 3D equilibrium solvent distributions in the presence of a static solute. While the quick convergence of solvent distributions of 3D-RISM is advantageous over explicit solvent sampling methods,[33] this advantage is increased orders of magnitude when dilute co-solvents are concerned, such as ammonia in the present study. It is this huge advantage of 3D-RISM/RISM that we seek to exploit with the pathway determination method presented here.

The *RismPath* algorithm constructed (details of algorithm are in the Methods section) was first validated by determining the water path for TrpCage, a fast-folding engineered microprotein that is often used as a test system in computational studies due to its small size but protein-like topology. For this system *RismPath* was used to calculate the most likely path water could traverse from a cavity inside the mini-protein to a point on the exterior near the N-terminal asparagine. The calculation revealed a resultant path of the 11-node *RismPath* calculation which is 17.61 Å in length and neatly traverses the perimeter of the excluded volume of the solute (Supporting Information Figure S2). The path appears qualitatively to traverse the minimum distance between the two end points without violating the solvent accessible surface. But since it is based on 3D-RISM/RISM data, it relies not on a geometrically defined surface area but rather on converged solvent−solute and solvent−solvent interactions.

Subsequently, the algorithm was validated for CPS synthetase, where the ammonia pathway has been elaborated via crystallography studies and later rigorously explored with both long classical MD and umbrella sampling simulations. Here, without utilizing prior knowledge of the pathway, *RismPath* was run on CPS using only the crystal structure with the end points as the small subunit active site and the carboxy phosphate intermediate active site. The calculation yielded a path length of 46.3 Å. The pathway, shown in Supporting Information Figure S3, is in qualitative agreement with the simulation studies that showed a multistep path. The success of *RismPath* on CPS suggests that it can determine pathways for systems with long, convoluted ammonia pathways such as in our target for this study, PurL. Finally, *RismPath* was used to identify the NH_3 pathway within WT PurL and to suggest validation experiments. Initially, *RismPath* was run on the crystal structure to determine a path between the gate formed by Phe1094 and Phe1165 in the glutaminase domain and the FGAR/ATP binding site. Unlike in the validation calculations for TrpCage and CPS, the algorithm failed to determine any pathway (after 500 trials). This suggests that the crystal structure, as-is, does not contain a complete, continuous pathway. However, it had already been suggested[34] that the introduction of fluctuations into the structure might be necessary to reveal the pathway.

To introduce fluctuations, the crystal structure was taken as an initial structure for an MD cascade with a 5 ns production run. *RismPath* was then run on 100 snapshots from the 5 ns run (every 50 ps) with otherwise identical parameters as for the crystal structure. Of the 100 snapshots, *RismPath* successfully determined a path for only 23. Comparing the nodes of the successful paths to the two possible purported pathways (path 1 or path 2), all 23 matched path 2. This suggests though the path is often obstructed, path 2 is the apparent viable path. Figure 1b shows the two purported paths from crystallography and the 23 *RismPath* pathways. To enable experimental testing of the "path 2" hypothesis, we designed several mutations which could potentially block it: S312W, S312V, S312I, S312L, S312F, A384F, A384I, A384L, A384V, V333F, V333I, and V333L.

We tested these mutations computationally based on the same procedure as the WT calculations. The mutations were performed in *tleap,* which were preceded by the identical MD cascade and *RismPath* parameters as the WT. Supporting Information Figure S4 shows the designed mutants in the context of the purported and apparent paths. According to the *RismPath* calculations on the MD snapshots, none of the mutants completely block path 2. Some, however, partially inhibit the path. Specifically, A384F and A384I only allowed 8% and 9% success of *RismPath*, respectively (compared to 23% in

DOI: 10.1021/cb501015r
ACS Chem. Biol. 2015, 10, 698−704

the WT) Table 1. Surprisingly, some mutations apparently induce a completely different path than both path 1 and path 2.

Table 1. Apparent Paths Determined by *RismPath* Calculations on PurL WT and Mutants

	% path success	path 1	path 2	path 3
WT	23	0	23	0
S312W	55	0	55	0
S312V	12	0	10	2
S312I	13	0	10	3
S312L	11	0	11	0
S312F	90	0	88	2
A384F	8	0	7	1
A384I	9	0	6	3
A384L	16	0	15	1
A384V	17	0	16	1
V333F	28	0	28	0
V333I	12	0	12	0
V333L	13	0	13	0

For about half the mutants, a minority of the successful paths lied along a third path (Path 3). Path 3 lies on the same side of the two helices as path 1, but is separated on average by about 9 Å. No calculations resulted in a path along purported path 1. As can be clearly seen (Supporting Information Figure S5), a third path clearly deviates from both initial purported paths. This result perturbs the initial hypothesis that path 2 is the "correct" path. Rather, it suggests that while path 2 may be the primary path, path 3 can serve as an auxiliary path when path 2 is blocked. Table 1 shows the path identity of calculations on the WT and mutants. The identity of the "apparent" path for each calculation was determined by the closest approach of each determined path and a central reference point unique to each of the three paths. For path 3, this reference point was taken directly from an arbitrary *RismPath* calculation result that was visually determined to be clearly distinct from paths 1 and 2.

To validate and develop insights, based on theoretical predictions, complementary experimental mutations were performed. The mutations in this region were made only along path 2, as that was the only path predicted to be permissible for ammonia passage. The flow of the ammonia was determined by calculating leakage of ammonia and by measuring FGAM synthetase activity following procedures detailed in the Supporting Information. The three positions where mutations were designed in accord with computational

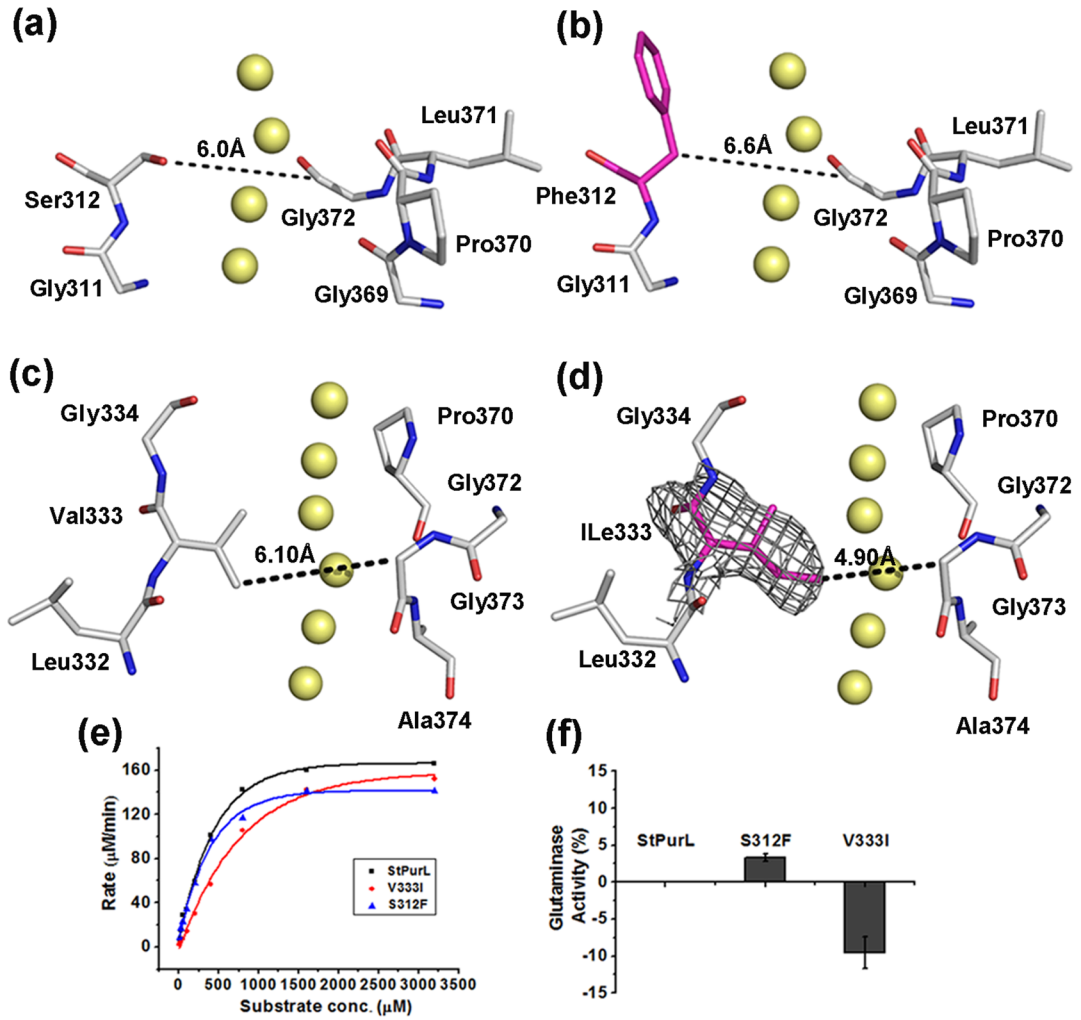

Figure 2. Mutations along path 2. (a) WT and (b) modeled S312F mutation showing greater path accessibility. (c) WT and (d) crystal structure of V333I mutant demonstrating path constriction ($F_o - F_c$ density is contoured at 3.0σ). (e) Data of FGAM synthetase activity and (f) percentage ammonia leakage of mutant proteins as compared to WT.

DOI: 10.1021/cb501015r
ACS Chem. Biol. 2015, 10, 698–704

data were Ser312, Val333, and Ala384. The computational studies predicted that mutations in position Ala384 with bulkier residues result in a maximum decrease in path accessibility and should affect ammonia channelling to the greatest extent. Experimental results show that replacing Ala384 with either phenylalanine residue, A384F, or by an isoleucine residue, A384I, was extremely deleterious to the protein and resulted in the protein going into inclusion bodies. It appears that this position is very sensitive to perturbation, and most likely these path blocking mutations severely constrict the path, causing serious clashes within the protein, thereby leading to protein instability.

Unlike the Ala384 position, mutations in Ser312 to bulkier residues like S312F and S312W were proposed by 3D-RISM/RISM calculations to exhibit a dramatic 90% path success rather than the 23% observed for the wild-type (Table 1). *In silico* mutation of S312F on the available structure revealed that replacement of a serine residue by a phenylalanine residue is well accommodated. The preferred phenylalanine rotamer, however, adopts a conformation that resides outside the channel, thereby increasing channel size (Figure 2a,b). Experimentally, the S312F and S312L mutants were stable (Supporting Information Figure S6) and possess FGAM synthetase activity at power with the wild type (Table 2).

Table 2. Kinetics Data for FGAM Synthetase Activity

protein	K_m (mM)	k_{cat} (s^{-1})	k_{cat}/K_m (M^{-1} s^{-1})
StPurL	0.27 ± 0.03	1.30 ± 0.08	4.9×10^3
V333I	0.48 ± 0.03	1.28 ± 0.14	2.6×10^3
S312F	0.26 ± 0.01	1.15 ± 0.03	4.4×10^3

This is most likely because the current existing path is able to deliver the ammonia produced without widening it. Even though the path is more accessible, the production of ammonia at the glutaminase active center or its consumption is independent of the path. Additionally, CD studies on S312F exhibited overall structural perturbations as signified by a lower ellipticity value compared to the wild type. The peak at 222 nm in the S312F mutant is also not properly curved, signifying a slight loss of α-helical structure (Supporting Information Figure S7a). Moreover, the thermal denaturation profile of S312F lacks the first transition, which is always observed in the wild type[27] (Supporting Information Figure S7b). Previously, the first transition was attributed to the unfolding of the N-terminal domain.[27] Hence, it appears that the mutation of S312F causes conformational frustration of phenylalanine residue, forcing it to adopt a rotamer that pushes the N-terminal domain outward, resulting in partial unfolding of this region, thereby yielding a lower ellipticity value. The slight rearrangement of the N-terminal domain may also lead to opening of path 3, and catalysis is therefore unaffected. On the other hand, experimentally constricting the path by carrying out a V333I mutation, predicted to reduce the path success rate by 50%, results in an analogous reduction of catalytic efficiency by 50% (Table2). The X-ray structure of the V333I mutant also shows that path 2 is now constricted by 1.2 Å (Table S2, Figure 2d).

It can be concluded that ammonia passage is now restricted due to the tunnel being partially blocked by a bulkier isoleucine residue (Figure 2c,d). Direct measurement of the ammonia released into the medium also asserts this claim as greater than 10% increase in ammonia leakage, compared to wild-type is observed in the V333I mutant protein (Figure 2f). It appears because of the constriction introduced that the ammonia (although being produced at the same rate as in wild-type (Supporting Information Figure S8)) is reaching the FGAM synthetase site at a slower rate, hence causing part of it to diffuse out of the protein.

In conclusion, here, we designed a computational solution to molecular path determination for PurL, where crystallographic data yielded two ambiguous pathways; "path 1" and "path 2." A computational algorithm, *RismPath*, was proposed, which exploits the 3D distribution of solvent and cosolvents in a channel, obtained from the 3D-RISM/RISM. The algorithm was validated by a benchmark-type calculation concerning the water pathway in the tryptophan cage. The new algorithm predicted "path 2" as the preferred mode of ammonia transfer and suggested a third, auxiliary path. The 3D-RISM/RISM calculation combined with the MD simulation reveals that the structural fluctuation is essential to open up a dominant "ADP" adjacent pathway. Supporting experimental studies validate the identity of the path and demonstrate that constricting the path in the central portion, far from the active centers, results in reduction of FGAM synthetase catalytic efficiency by 50%. Whereas, widening the path has no effect on function. This signifies that the residues in the middle of the channel do not partake in catalytic coupling and serve only as channel walls facilitating ammonia transfer.

METHODS

Theoretical Analysis. An algorithm (*RismPath*) is designed here which determines the most likely pathway between two given end points utilizing 3D-RISM distribution functions. *RismPath* first generates 3D distribution functions using 3D-RISM that represent a probability map for each effectively unique atomic site on each solvent molecule. Only the distribution of a single representative site is utilized to detect the pathway. The site of a central atom such as O in H_2O or N in NH_3 is used. Given a set of pathway end points, the algorithm determines the most favorable path energetically in terms of the distribution of the target atom. *RismPath* (Supporting Information Figure S1) begins by interpolating a linear path between the two end points containing a set of discrete "nodes." Since the site distribution inside a biomolecule contains many obstructions, the position of these intermediate nodes often lies within extremely unfavorable locations (such as within the excluded volume of the protein). So the nodes are then jiggled perpendicularly to the path vector until each lies in a location with nonzero probability. Since, this stochastic jiggling can overextend the path (e.g., extending outside the protein), the paths of such cases are discarded and the process restarted. Otherwise, if the path is not too long, it is then subjected to steepest descent minimization using "elastic band-type" potential according to the equations below.[35]

$$E^{\text{total}} = E^{\text{PMF}} + E^{\text{band}} \tag{1}$$

$$E^{\text{PMF}} = \sum_{i=2}^{N-1} -k_B T \ln(g(\mathbf{r}_i)) \tag{2}$$

$$E^{\text{band}} = \frac{k}{4} \sum_{i=2}^{N-1} [(\bar{d}_0 - d_{i,i+1})^2 + (\bar{d}_0 - d_{i,i-1})^2] \tag{3}$$

Here, E^{PMF} is the sum of the potentials of mean force from probability distribution of the solvent site at each node. E^{band} is a spring-like potential used to maintain an even spacing between each node. N is the total number of nodes on the path including the end points. d is the distance between the nodes indicated by the subscripts, and $\bar{d}_0$ is the average node−node distance. k is a tunable spring constant. After minimization, additional interstitial nodes are interpolated linearly between the existing nodes to increase the continuity of the path. This

DOI: 10.1021/cb501015r
ACS Chem. Biol. 2015, 10, 698−704

entire procedure is repeated a set number of trials after which the path with the lowest E^{total} is reported. Parameters for production calculations were tuned (*calculation parameters* in SI) such that the stochastic algorithm consistently yields the same result of either "path" or "fail" for the same input systems.

To validate the *RismPath* algorithm on three different systems like TrpCage, CPS, and PurL, many other system parameters and calculation parameters of 1D-RISM and 3D-RISM are used. The detailed descriptions of the parameters are described in the Supporting Information.

EXPERIMENTAL METHODS

Cloning, Expression, and Purification. Point mutants of the enzyme were made by site directed mutagenesis (SDM) using the strategy employed by the Quikchange (Stratagene) kits. In cases where this strategy failed, overlap and extension PCR followed by cloning using *Kpn*I and *Bam*HI restriction enzymes was employed. All the proteins were expressed and purified by the previously described procedure.[27]

X-ray Crystallography. Diffraction data for V333I were collected on Rigaku FR-E+ super bright microfocus rotating anode at the National Institute of Immunology (Delhi, India). The V333I crystals were grown by hanging drop vapor diffusion as described previously.[25] Data were collected using an R AXIS IV++ detector, 1.0° oscillation, 3 min exposure time, and 240 mm crystal to detector distance at a wavelength of 1.54 Å. The data were processed using HKL 2000.[36] The structure was determined by performing molecular replacement using the native StPurL structure (PDB ID IT3T) and refined using CNS.[37] All manual model building was performed using the program Coot.[38] The crystallographic data statistics are shown in Supporting Information Table S2.

Biophysical Characterization. The secondary structure analysis and thermal denaturation experiment of wild type and mutant proteins were performed by the previously described method[27] mentioned in the Supporting Information.

Enzyme Assays. The other biochemical assays (FGAM synthetase assay and glutamate dehydrogenase assay) to measure the activity of proteins are clearly described in the Supporting Information.

ASSOCIATED CONTENT

Supporting Information

Additional materials and methods, Figures S1−S8, Tables S1 and S2, and references for supporting data. This material is available free of charge via the Internet at http://pubs.acs.org.

Accession Codes

Coordinates and structure factors have been deposited in the Protein Data Bank with accession numbers 4R7G for the V333I mutant structure.

AUTHOR INFORMATION

Corresponding Authors

*E-mail: hirataf@fc.ritsumei.ac.jp.

*E-mail: ruchi@chem.iitb.ac.in. Phone: +91-22-25767165.

Present Address

[‖]Schrödinger, Inc., 120 West 45th Street, 17th Floor, New York, New York 10036.

Author Contributions

[§]These authors have equally contributed to this work.

Notes

The authors declare no competing financial interests.

ACKNOWLEDGMENTS

We thank Prof. S. E. Ealick of Cornell University and Prof. J. Stubbe of MIT for providing the FGAR for the experiments. We also thank DST [Grant No. DST/INT/SOUTH AFRICA/P-04/2014] for support. We additionally thank National Institute of Immunology, India for providing the X-ray Facility.

REFERENCES

(1) Miles, E. W., Rhee, S., and Davies, D. R. (1999) The Molecular Basis of Substrate Channeling. *J. Biol. Chem. 274*, 12193−12196.

(2) Huang, X., Holden, H. M., and Raushel, F. M. (2001) Channeling of Substrates and Intermediates in Enzyme-Catalyzed Reactions. *Annu. Rev. Biochem. 70*, 149−180.

(3) Milani, M., Pesce, A., Bolognesi, M., Bocedi, A., and Ascenzi, P. (2003) Substrate channeling: Molecular bases. *Biochem. Mol. Biol. Educ. 31*, 228−233.

(4) Spivey, H. O., and Ovádi, J. (1999) Substrate Channeling. *Methods 19*, 306−321.

(5) Mouilleron, S., and Golinelli-Pimpaneau, B. (2007) Conformational changes in ammonia-channeling glutamine amidotransferases. *Curr. Opin. Struct. Biol. 17*, 653−664.

(6) Raushel, F. M., Thoden, J. B., and Holden, H. M. (1999) The Amidotransferase Family of Enzymes: Molecular Machines for the Production and Delivery of Ammonia. *Biochemistry 38*, 7891−7899.

(7) Massiere, F., and Badet-Denisot, M. A. (1998) The mechanism of glutamine-dependent amidotransferases. *Cell. Mol. Life Sci. 54*, 205−222.

(8) Zalkin, H., and Smith, J. L. (1998) Enzymes utilizing glutamine as an amide donor. *Adv. Enzymol. 72*, 87−144.

(9) Thoden, J. B., Holden, H. M., Wesenberg, G., Raushel, F. M., and Rayment, I. (1997) Structure of Carbamoyl Phosphate Synthetase: A Journey of 96 Å from Substrate to Product. *Biochemistry 36*, 6305−6316.

(10) Krahn, J. M., Kim, J. H., Burns, M. R., Parry, R. J., Zalkin, H., and Smith, J. L. (1997) Coupled Formation of an Amidotransferase Interdomain Ammonia Channel and a Phosphoribosyltransferase Active Site. *Biochemistry 36*, 11061−11068.

(11) Binda, C., Bossi, R. T., Wakatsuki, S., Arzt, S., Coda, A., Curti, B., Vanoni, M. A., and Mattevi, A. (2000) Cross-talk and ammonia channeling between active centers in the unexpected domain arrangement of glutamate synthase. *Structure 8*, 1299−1308.

(12) List, F., Vega, M. C., Razeto, A., Hager, M. C., Sterner, R., and Wilmanns, M. (2012) Catalysis Uncoupling in a Glutamine Amidotransferase Bienzyme by Unblocking the Glutaminase Active Site. *Chem. Biol. 19*, 1589−1599.

(13) Thoden, J. B., Huang, X., Raushel, F. M., and Holden, H. M. (2002) Carbamoyl-phosphate Synthetase: Creation of an Escape Route for Ammonia. *J. Biol. Chem. 277*, 39722−39727.

(14) Bera, A. K., Smith, J. L., and Zalkin, H. (2000) Dual Role for the Glutamine Phosphoribosylpyrophosphate Amidotransferase Ammonia Channel: Interdomain Signaling and Intermediate Channeling. *J. Biol. Chem. 275*, 7975−7979.

(15) Petrek, M., Otyepka, M., Banas, P., Kosinova, P., Koca, J., and Damborsky, J. (2006) CAVER: a new tool to explore routes from protein clefts, pockets and cavities. *BMC Bioinf. 7*, 316.

(16) Petřek, M., Košinová, P., Koča, J., and Otyepka, M. (2007) MOLE: A Voronoi Diagram-Based Explorer of Molecular Channels, Pores, and Tunnels. *Structure 15*, 1357−1363.

(17) Yaffe, E., Fishelovitch D Fau - Wolfson, H. J., Wolfson Hj Fau - Halperin, D., Halperin D Fau - Nussinov, R., and Nussinov, R. (2008) MolAxis: efficient and accurate identification of channels in macromolecules. *Proteins 73*, 72−86.

(18) Fatemeh Khalili-Araghi, J. G., Wen, P.-C., and Marcos Sotomayor, E. T. A. K. S. (2009) Molecular dynamics simulations of membrane channels and transporters. *Curr. Opin. Struct. Biol. 19*, 128−137.

(19) Fan, Y., Lund, L., Yang, L., Raushel, F. M., and Gao, Y.-Q. (2008) Mechanism for the Transport of Ammonia within Carbamoyl Phosphate Synthetase Determined by Molecular Dynamics Simulations. *Biochemistry 47*, 2935−2944.

(20) Amaro, R., and Luthey-Schulten, Z. (2004) Molecular dynamics simulations of substrate channeling through an $\alpha-\beta$ barrel protein. *Chem. Phys. 307*, 147−155.

DOI: 10.1021/cb501015r
ACS Chem. Biol. 2015, 10, 698−704

(21) Kovalenko, A., and Hirata, F. (1998) Three-Dimensional Density Profiles of Water in Contact with a Solute of Arbitrary Shape: a RISM Approach. *Chem. Phys. Lett. 290*, 237−244.
(22) Beglov, D., and Roux, B. (1997) An Integral Equation to Describe the Solvation of Polar Molecules in Liquid Water. *J. Phys. Chem. B 101*, 7821−7826.
(23) Jorgensen, W. L., Chandrasekhar, J., Madura, J. D., Impey, R. W., and Klein, M. L. (1983) Comparison of simple potential functions for simulating liquid water. *J. Chem. Phys. 79*, 926−935.
(24) Berendsen, H. J. C., Grigera, J. R., and Straatsma, T. P. (1987) The Missing Term in Effective Pair Potentials. *J. Phys. Chem. 91*, 6269−6271.
(25) Anand, R., Hoskins, A. A., Stubbe, J., and Ealick, S. E. (2004) Domain Organization of Salmonella typhimurium Formylglycinamide Ribonucleotide Amidotransferase Revealed by X-ray Crystallography. *Biochemistry 43*, 10328−10342.
(26) Tanwar, A. S., Morar, M., Panjikar, S., and Anand, R. (2012) Formylglycinamide ribonucleotide amidotransferase from Salmonella typhimurium: role of ATP complexation and the glutaminase domain in catalytic coupling. *Acta Crystallogr., Sect. D: Biol. Crystallogr. 68*, 627−636.
(27) Tanwar, A. S., Goyal, V. D., Choudhary, D., Panjikar, S., and Anand, R. (2013) Importance of hydrophobic cavities in allosteric regulation of formylglycinamide synthetase: insight from xenon trapping and statistical coupling analysis. *PLoS One 11*, e77781.
(28) Hirata, F. (2003) *Molecular Theory of Solvation*, Kluwer Academic Pub., Dordrecht, The Netherlands, Vol. *24*.
(29) Kovalenko, A., and Hirata, F. (1999) Self-consistent description of a metal−water interface by the Kohn−Sham density functional theory and the three-dimensional reference interaction site model. *J. Chem. Phys. 110*, 10095.
(30) Kovalenko, A., and Hirata, F. (1999) Potential of Mean Force between Two Molecular Ions in a Polar Molecular Solvent: A Study by the Three-Dimensional Reference Interaction Site Model. *J. Phys. Chem. B 103*, 7942−7957.
(31) Perkyns, J., and Pettitt, B. M. (1992) A site−site theory for finite concentration saline solutions. *J. Chem. Phys. 97*, 7656−7666.
(32) Perkyns, J. S., and Montgomery Pettitt, B. (1992) A dielectrically consistent interaction site theory for solvent−electrolyte mixtures. *Chem. Phys. Lett. 190*, 626−630.
(33) Stumpe, M. C., Blinov, N., Wishart, D., Kovalenko, A., and Pande, V. S. (2010) Calculation of Local Water Densities in Biological Systems: a Comparison of Molecular Dynamics Simulations and the 3D-RISM-KH Molecular Theory of Solvation. *J. Phys. Chem. B 115*, 319−328.
(34) Jónsson, H., Mills, G., and Jacobsen, K. W. (1998) Nudged elastic band method for finding minimum energy paths of transition in classical and quantum dynamics in condensed phase simulations, (ed. Berne, G. C. a. D. F. C.), World Scientific, pp 385−404.
(35) Elber, R., and Karplus, M. (1987) A method for determining reaction paths in large molecules: Application to myoglobin. *Chem. Phys. Lett. 139*, 375−380.
(36) Otwinowski, Z., and Minor, W. (1997) Processing of X-ray Diffraction Data Collected in Oscillation Mod. *Methods Enzymol. 276*, 307.
(37) Brunger, A. T., Adams, P. D., Clore, G. M., DeLano, W. L., Gros, P., Grosse-Kunstleve, R. W., J, J. S., K, J., Nilges, M., Pannu, N. S., Read, R. J., Rice, L. M., Simonson, T., and Warren, G. L. (1998) Crystallography & NMR system: A new software suite for macromolecular structure determination. *Acta Crystallogr., Sect. D: Biol. Crystallogr. 54*, 904−921.
(38) Emsley, P., L, B., Scott, W. G., and Cowtan, K. (2010) Features and development of Coot. *Acta Crystallogr., Sect. D 66*, 486−501.

DOI: 10.1021/cb501015r
ACS Chem. Biol. 2015, 10, 698−704